HAL
open science

Modeling the pressure generation in aluminum based thermites

Vincent Baijot, Ludovic Glavier, Jean-Marie Ducéré, Mehdi Djafari-Rouhani, Carole Rossi, Alain Estève

To cite this version:

Vincent Baijot, Ludovic Glavier, Jean-Marie Ducéré, Mehdi Djafari-Rouhani, Carole Rossi, et al.. Modeling the pressure generation in aluminum based thermites. Propellants, Explosives, Pyrotechnics, Wiley-VCH Verlag, 2015, 40 (3), pp. 402-412. hal-01094520

HAL Id: hal-01094520

https://hal.archives-ouvertes.fr/hal-01094520

Submitted on 16 Dec 2014

HAL is a multi-disciplinary open access archive for the deposit and dissemination of scientific research documents, whether they are published or not. The documents may come from teaching and research institutions in France or abroad, or from public or private research centers.

L'archive ouverte pluridisciplinaire **HAL**, est destinée au dépôt et à la diffusion de documents scientifiques de niveau recherche, publiés ou non, émanant des établissements d'enseignement et de recherche français ou étrangers, des laboratoires publics ou privés.

Propellants,
Explosives,
Pyrotechnics

Full Paper

DOI: 10.1002/prep.201((full DOI will be filled in by the editorial staff))

Modeling the pressure generation in aluminum based thermites

V. Baijot[a], L. Glavier[a], J.M. Ducéré[a], M. Djafari Rouhani[a], C. Rossi[a], A. Estève[a]*

CNRS; LAAS; 7 avenue du colonel Roche, 31031 Toulouse, France
Université de Toulouse; UPS, INSA, INP, ISAE, LAAS; F-31077 Toulouse, France

Abstract:

The paper proposes a new theoretical model based on local thermodynamic equilibrium enabling the prediction of gas generation during the reaction of aluminum-based thermites. We demonstrate that the model has the capability to predict the total pressure and its partial pressure components as a function of the reaction extent and compaction. Al/CuO, Al/Bi_2O_3, Al/Sb_2O_3, Al/MoO_3 and Al/WO_3 thermites are modeled and their capability to generate pressure compared. Simulation results are also validatedthrough dedicated experiments and showgeneral agreement beyond the state of the art. Mechanisms underlying pressure generation are detailed. A two-stage process for the pressure increase in Al/CuO reaction,also observed experimentally,is shown to be driven by oxygen generation as produced byCuO and Cu_2O vaporizationthrough different kinetics. Comparison with experiment stresses the issue of the understanding of the complex chemical processes taking place during vaporization and subsequent gas phase reactions and the need to determine their thermodynamicconstants.

Keywords:thermite, pressure generator, Al/CuO, Al/Bi_2O_3, Al/Sb_2O_3, Al/MoO_3, Al/WO_3

1 Introduction

Alumino-thermite materials represent an interesting class of energetic substancesnotably because of their high energy densities, adiabatic flame temperature, and when nanosized, high reaction rates. Alumino-thermite is an oxydo-reduction reaction involvinga metal (fuel) and a metallic oxide (or possibly a non-metallic oxide) to form a stable product after reaction.

Thermites materials have been actively investigated for a wide range of potential applications including railroad welding, materials processing to form refractory materials, additives in propellants, explosives and pyrotechnics [1-3] and more recently also for micro initiation[4-20], environmentally clean primers, in situ welding [21].

Among numerous possible exothermic metal/oxide couples listed in [22], the most investigated ones mix Al with MoO_3, CuO, Bi_2O_3, Fe_2O_3, MnO_2, WO_3, I_2O_5. For the last two decades most of the research efforts aimed at reducing metal and oxide components size, improving their intimacy, to increase the reaction rate and decrease the ignition delay while improving safety.

More recently, thermite materials were also considered to produce gas species or pressure bursts opening new potential fields of applications as pressure mediated molecular delivery [23, 24], biological agent inactivation [25-27], hydrogen production[28, 29] or propulsion systems [7-9] .

A few teams demonstrated experimentally that Al/Bi_2O_3 and, to a lesser extent, Al/I_2O_5 mixtures generate the highest pressure pulses[27, 30, 31]in comparison with other thermite couples. Martirosyan[31]considered that the reaction product (bismuth or iodine) boils at a temperature of 1560°C and 184°C, respectively, that is lower than the maximum reaction temperature, causing bismuth or iodine evaporation with subsequent increase of the released gas pressure.
For some thermites as Al/CuO, experiments using time-resolved mass spectrometry have measured significant O_2release, undergo rapid heating [32-33].The formation of gaseous intermediates and their contribution to the pressurization may suggest why a system such as Al/MoO_3, which is thermodynamically predicted to produce approximately only the percent of the gas that Al/CuO or Al/Bi_2O_3 does, can still react rapidly and exhibit pressures as the other thermites.

Despite these experimental research investigations, the effects of thermite composition, packing densitytogether with its environmental conditions on the gas production (type and repartition of produced species and rate of gas release) need to be studied and understood in greater details.On the theoretical side, a first attempt to simulate thermite pressure release was published by K. Martirosyan*et al.*[34]. They proposed to solve numerically the equations of

gas dynamics.Apreliminary study by the authors showed systematic overestimation of the calculated generated pressures[35]. Our goal is to bring the simulation closer to the actual chemical processes that may occur during reaction including gas phase interactions, vaporization and condensation processes.

The aim of the present work is to propose a new generic model, based on thermodynamic considerations, able to predict the maximum reaction pressure, temperature and reaction end products (gas and solid formed species) as a function of the overall extent of reaction and packing density.

This theoretical tool makes it possible to establishquantitatively a hierarchy of alumino-thermite couples in relation to applicative requirements, specifically concerning pressure and gas delivery.

The paper is organized as the following. Section 2 is dedicated to the model description.Simulation results are reported in section 3 starting with a case study on Al/CuO followed by a comparison with other materials, namely Al/MoO_3, Al/Bi_2O_3, Al/WO_3 and Al/Sb_2O_3. For all of them, the maximum pressure, temperature and reaction products are given as a function of the extent of reaction and the percentageof Theoretical Maximum Density (TMD). In section4, theoretical results are compared with experimental data allowing the validation and discussion of the theoretical approach before concluding and giving some perspectives in section5.

2 Model description

For Al based thermites, the reaction can be written as:

$$\frac{2.b}{3}\mathrm{Al} + \mathrm{M_a O_b} \rightarrow \frac{b}{3}\mathrm{Al_2O_3} + \mathrm{a\,M} \qquad (1)$$

whereM_aO_b is the metal oxide corresponding to the metal M with valency 2b/a.

Equation (1) is only a schematic representation of mechanisms occurring during thermite reaction. Indeed, in most practical cases, various intermediates and end products, such as oxides, sub-oxides and alloys, may be encountered during the reaction process. All possible phases are not well known and characterized experimentally. A theoretical approach would require a thorough investigation, using quantum chemical methods, of all possible intermediates and end products, including metastable phases and metallic aggregates. This is not the purpose of this paper where only the most documented compounds are considered.

A combustion process is basically an out of equilibrium process. But, an accurate kinetic model should necessarily include the various kinetic constants associated with various phase transitions that are not available today. On the other hand, the high temperatures reached during the reaction enhance the reactions towards the thermodynamic equilibrium. For this reason, and in the absence of available thermodynamic data on possible intermediates and end products, we will confine our model to the thermodynamic equilibrium. However, in order to get insight into the temporal evolution of the reaction process, we introduce the extent of reaction parameter ξ ranging from 0 to 1. The extent of reaction is not proportional to the time, since the reaction rates increase with the temperature. But, at least, the extent of reaction is a monotonically increasing function of time.

In our model, we consider stoichiometric mixture (no excess of Al) and assume that the thermodynamic equilibrium is temporarily reached for each value of the extent of reaction, although the global equilibrium is only reached at the end of the reaction. This is equivalent to the usual assumption of local thermodynamic equilibrium in the treatment of irreversible processes. The schematic reaction represented in Eq. (1) can now be reformulated as:

$$\frac{2.b}{3}\mathrm{Al} + \mathrm{M_a O_b} \rightarrow \frac{b\xi}{3}\mathrm{Al_2O_3} + \mathrm{a}.\xi\,\mathrm{M} + (1-\xi).\frac{2.b}{3}\,\mathrm{Al} + (1-\xi)\mathrm{M_a O_b} \qquad (2)$$

whereξrepresents the fraction of thermite converted, while the remaining$(1-\xi)$ fraction is still in its initial form.

At this stage, additional phases are introduced into equation (2), depending on the nature of the oxide, the actual temperature and the different vapor partial pressures in the reaction chamber.

These phases result from:
- the melting and boiling of all species,
- the decomposition of alloys and oxides,
- the condensation in alloy or oxide forms.

All thermodynamicsconstants, including formation energies, concerning these phases are taken from the literatureand the main ones are reported in Tables1.a and 1.b. The free energies are preferred to enthalpies since all of the experiments to validate the model are performed in a constant volume pressurized chamber.

Table 1.a:Specific heat of thermite reaction.

Thermite couple	Specific heat of reaction (kJ/cm^3)
Al/CuO	20.6
Al/WO_3	15.6
Al/MoO_3	18.0
Al/Bi_2O_3	15.0
Al/Sb_2O_3	10.6

Table 1.b: Latentheatsof vaporization/decomposition at atmospheric pressure.

Boiling species	Latent heat of vaporization (kJ/mol)
Al Vaporization	294
Al_2O_3Decomposition	1402
Cu Vaporization	338

CuODecomposition	70
Cu_2O Decomposition	115
W Vaporization	800
WO_2Decomposition	534
WO_3Decomposition	230
Bi Vaporization	151
Bi_2O_3Decomposition	573
Mo Vaporization	600
MoO_3 Vaporization	138
Sb Vaporization	166
Sb_2O_3 Decomposition	644

In most cases, both the boiling points and the partial vapor pressures reported in the literature correspond to atmospheric pressures or less. In order to obtain boiling points at high pressures such as the ones reached in confined thermite reactions, we have extrapolated these values to higher pressures using the following expression:

$$P_i(T) = K_i \times T^{3/2} \times \exp^{\left(-\frac{\Delta U_i}{k_B T}\right)} \quad (3)$$

where$P_i(T)$is the partial pressure of the gas specie i at the temperature T and ΔU_iits vaporization energy. $k_B$is the Boltzmann constant. Equation (3) can either be deduced from the kinetic theory of gases or by equating the chemical potentials of species in the gas phase and in the condensed phase. In equation (3), the entropic part of the free energy, resulting from the thermal motion of atoms and molecules, is contained in the pre-exponential factor K_i and the internal energy appears in the exponent. Both theoretical approaches lead to the constant K_i:

$$K_i = \frac{\sqrt{2\pi m_i {k_B}^3}}{s_i h} \quad (4)$$

where$m_i$is the molecular mass of the specie*i*. s_i the area of its surface unit cell (in the condensed phase), and $h$is the Plank constant. However, in our model, we have considered the constants K_i as adjustable parameters and have fitted them to experimental boiling points at atmospheric pressure. The vaporization energies ΔU_i correspond to the formation of elemental metallic atoms and O_2 molecules in the gas phase, except for MoO_3 which evaporates in its molecular form. The perfect gas law is adopted for all species in the gas phase.

The simulation procedure follows closely the experiments performed for the validation of the model. In these experiments, the reaction chamber is filled with a given amount of thermite, i.e. a given TMD percentage. We should notice that the chamber can never be completely filled such that the maximum experimental %TMD is 50%. For a given thermite Al/M_aO_b and %TMD, we first choose a value of the extent of reaction ξ and scan the temperature from ambient to 4000°C. The partial pressures of various species are then calculated at each temperature using equation (4) and the number of molecules determined from the perfect gas law. The composition of the condensed phase is then deduced by subtraction. We remind that, in these experiments, the volume of the condensed phase is not small compared to the total volume of the reaction chamber. It is therefore necessary to take it into account when applying the perfect gas law.

The equation of conservation of energy is applied to determine the actual temperatures as a function of extent of reactionξ. The heat released by the reaction is equal to$\xi.\tau.Q$, withτbeing the %TMD and Q the specific heat of reaction (see Table 1.a). This heat is used to increase the temperature of the system and to supply the latent heats required for the phase transitions. The overall heat quantity $q(T)$ required to heat the system to the desired temperature T can be formulated as:

$$q(T) = \int_{T_0}^{T} [C_v(T) + h(T)].dT \quad (5)$$

Where T_0 is the initial temperature, taken here as the ambient temperature (25°C). $C_v(T)$is the temperature dependent heat capacity of the whole system and $h(T)$the latent heat. The function $h(T)$is composed of a series of Dirac delta functions, at appropriate temperatures, for all phase transitions, except the vaporization considered as a continuous process, in relation with partial vapor pressures. The temperature dependent heat capacities, for all species, are taken from the literature [36-38], and interpolated before integration. In the temperature ranges where the data are not available, particularly at high temperatures, we use $3k_BT$for each atom in the solid phase or MoO_3 molecule in the gas phase, $\frac{3}{2}k_BT$ and $\frac{5}{2}k_BT$ for each metallic atom in the gas phase and each O_2 molecule, respectively. These expressions are taken from Einstein's law for solids at high temperatures, and from the kinetic theory of gases for monovalent and divalent molecules. The various heat capacities are finally added to find the total $C_v(T)$.

Scanning the temperature range upwards, *q(T)* is an increasing function of the temperature. It reaches the heat released by the reaction at some value of T, which is the actual temperature reached at a given extent of reaction.

In this paper, all heat losses are neglected since they depend strongly on the size of the reaction chamber. In a previous paper [35], we have evaluated the heat losses during the pressure rise, for all experiments used to validate the model, and have shown that they are always negligible with respect to the released heat of reaction.

3Results

3.1 Al/CuO case study

Al/CuO is one of the most frequently used thermite in practical applications as well as among the most documented one. For this reason, we start by describing in detail the implementation of our model to the Al/CuO case, before presenting a more general

overview of the results obtained for four other thermites. For Al/CuO, the schematic reaction expressed in equation (1) can be broken into nine reactions contained in the six following equations, and taken into account in our simulations.

$$2\,\mathrm{CuO}_{(s)} \leftrightarrow \mathrm{Cu_2O}_{(s)} + \frac{1}{2}\mathrm{O}_{2\,(g)}$$

$$\mathrm{Cu_2O}_{(s)} \xrightarrow{1244\ °C} \mathrm{Cu_2O}_{(l)} \leftrightarrow 2\,Cu_{(l)} + \frac{1}{2}\mathrm{O}_{2\,(g)}$$

$$\mathrm{Cu}_{(s)} \xrightarrow{1085\ °C} \mathrm{Cu}_{(\mathrm{l})} \leftrightarrow 2\,Cu_{(g)}$$

$$\mathrm{Al_2O_{3\,(s)}} \xrightarrow{2072\ °C} \mathrm{Al_2O_{3\,(l)}} \leftrightarrow 2Al_{(g)} + \frac{3}{2}\mathrm{O}_{2\,(g)}$$

$$\mathrm{Al}_{(s)} \xrightarrow{660\ °C} \mathrm{Al}_{(l)} \leftrightarrow \mathrm{Al}_{(g)}$$

In these equations, the subscripts *(s)*, *(l)* and *(g)* stand for solid, liquid and gas phases respectively. Among these nine reactions, four are phase transitions between condensed phases, represented by direct reactions. A transition temperature is systematically assigned to each of them. The five remaining reactions are reversible (as indicated by the reverse arrows), with the presence of a gas phase. The driving force balancing the direct or reverse reaction is the partial vapor pressure in the gas phase.

As described in section 2, the equilibrium temperature is calculated for each value of ξ. The calculated temperatures are independent of TMD percentage since both the released reaction heat and the heat necessary to increase the temperature are proportional to %TMD. As a consequence, temperature splitting as a function of %TMD, may appear as a result of heat losses that are neglected at this point. The Al/CuOequilibrium temperatures as a function of ξ are reported in Fig. 1. We observe that, for Al/CuO, the equilibrium temperature increases up to 3400°C with a slight plateau at 2072°C corresponding toAl_2O_3 melting. Fig. 1 shows the maximum pressures for three different TMD percentages(10%, 30% and 50%). Themaximum pressure depends on the temperature, but also on the volume available for the expansion of the gas. Increasing the %TMD leads to a decrease of the free volume and an increase of the total pressure. For all three %TMD values, the pressure rise starts at ξ = 0.3, corresponding to a temperature around 1000°C (see Fig. 1), corresponding to the Al/CuO reaction onset.

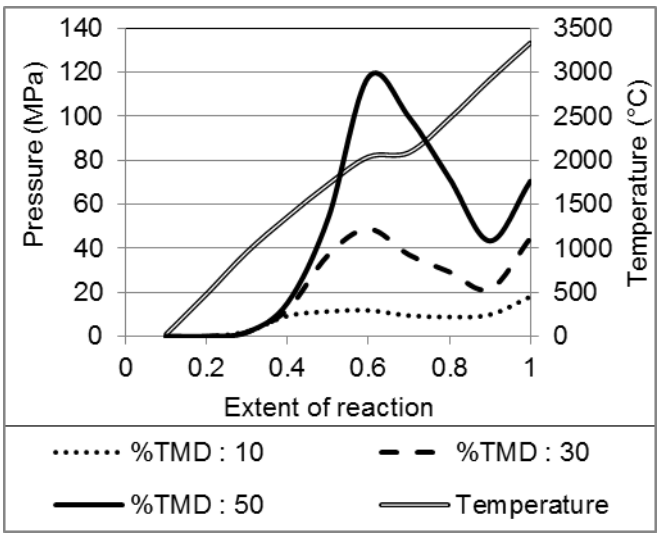

Fig. 1: Theoretical pressures, for different %TMD, and the equilibrium temperature, as a function of extent of reaction, during Al/CuO combustion.

We can further observe that the pressure rise is not monotonic such that the maximum pressure is reached when the reaction is still incomplete. This result is against the general belief that the pressure drop is only a consequence of reaction stop and subsequent cooling of the system through heat losses. Moreover, for low compaction (%TMD=30), the pressure evolution shows clearly an oscillating behavior. This trend can also be observed for higher compaction rate, although the first maximum is less pronounced and rather replaced by a shoulder.

To explain this behavior, we have plotted in Fig. 2, Al, Cu and O_2 partial pressures in the gas phase, together with the total pressure and the temperature, as a function of ξ and for a TMD percentage of 30%. Fig. 2 shows clearly that all partial pressures do not rise simultaneously. This results from the variety of their specific vapor pressures dependence against the temperature.

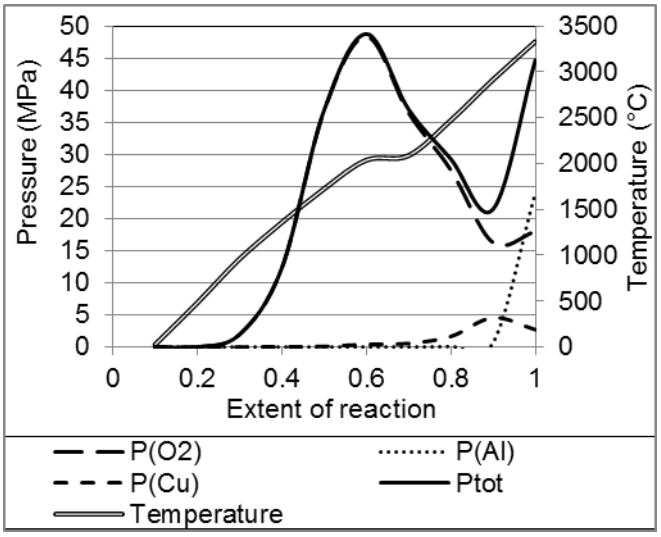

Fig. 2: Theoretical partial pressures together with the total pressure and the temperature, as a function of extent of reaction and for TMD percentage of 30%.

As observed in experiments [33], wesee in Fig. 2 that the total pressure is mainly driven by the oxygen gas phase which shows a first pressure peak at $\xi = 0.6$ and a gentle pressure shoulder at $\xi = 0.8$, resulting from the decomposition of CuO and Cu_2O, respectively. Aluminum and, to a much lesser extent, copper gas phases only impact the end of the reaction process. The Cu vapor comes from the evaporation of liquid Cu, while Al vapor comes from the decomposition of Al_2O_3. The latter process explains the increase of the total pressure observed from $\xi = 0.9$ to $\xi = 1$ (see Fig. 2). This results from the vaporization of Al_2O_3 due to the high final temperature (3330°C) that is superior to the decomposition temperature of the alumina (2977°C). When the reaction is near completion, the total pressure behavior is almost entirely governed by the aluminum partial pressure. The oxygen partial pressure stabilizes due to compensation between vaporization of the liquid alumina providing oxygen molecules and oxidation reaction with aluminum.

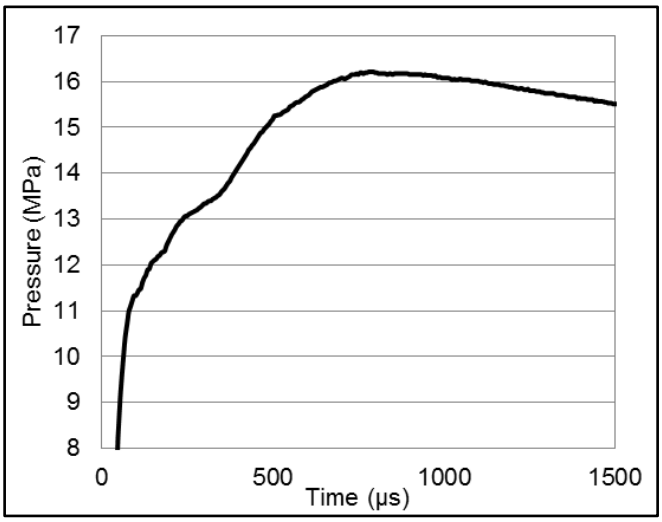

Fig. 3: Experimental Al/CuO pressure versus time at 30 %TMD[35].

Similar pressure evolution tendency, i.e. a peak and a shoulder, has also been found experimentally (see Fig. 3). But, the positions of the peak and the shoulder are reversed. The reason is the relative intensities of the two oxygen peaks. Calculated oxygen partial pressure coming from the decomposition of CuO is too high because of its lower latent heat of vaporization (see Table 1 b.This first peak replaces therefore the experimental shoulder, but hides, in turn, the real experimental peak.

To summarize, for 10 %TMD, the pressure saturation is reached at the end of the reaction (ξ=1) giving rise to a pressure saturation plateau around18 MPa. For 30 and 50 %TMD, maximum pressures of 49 and 118 MPa are obtained at an extent of reactionξ =0.6. From these maximum pressure values, the pressure decreases up to ξ =0.9 where the high temperature reached by the system causes the alumina to decompose and in consequence, the pressure to increase again, up to a value of71 MPa.

3.2Applications to other thermites

In this sectionfour other thermitecouples among the most widely studied (Al/Sb_2O_3, Al/Bi_2O_3, Al/MoO_3 and Al/WO_3) areanalyzedand their capability to generate gases and pressure compared. As previously indicated, a number of phase transitions are considered for the species involved ineach thermite reaction as summarized in Table 2.

Table 2:Phase transitions considered in the model for Al/Bi_2O_3, Al/MoO_3,Al/Sb_2O_3 and Al/WO_3 thermites (note that CuO phase transitions are detailed in the previous section 3.1).

Materials	T (°C)	Phase transition	Species
Al_2O_3	2042	Melting	$Al_2O_{3(s)}$, $Al_2O_{3(l)}$
Al_2O_3	2977	Decomposition	$Al_2O_{3(l)}$, $Al_{(g)}$, $O_{2(g)}$
Bi	272	Melting	$Bi_{(s)}$, $Bi_{(l)}$
Bi	1564	Vaporization	$Bi_{(l)}$, $Bi_{(g)}$
Sb	357	Melting	$Sb_{(s)}$, $Sb_{(l)}$
Sb	1314	Vaporization	$Sb_{(l)}$, $Sb_{(g)}$
Mo	2623	Melting	$Mo_{(s)}$, $Mo_{(l)}$
Mo	4639	Vaporization	$Mo_{(l)}$, $Mo_{(g)}$
W	3422	Melting	$W_{(s)}$, $W_{(l)}$
W	5663	Vaporization	$W_{(l)}$, $W_{(g)}$
Al	660	Melting	$Al_{(s)}$, $Al_{(l)}$
Al	2519	Vaporization	$Al_{(l)}$, $Al_{(g)}$
Sb_2O_3	655	Melting	$Sb_2O_{3(s)}$, $Sb_2O_{3(l)}$
Sb_2O_3	1425	Decomposition	$Sb_2O_{3(l)}$, $Sb_{(g)}$, $O_{2(g)}$
WO_3	1200	Melting	$WO_{3(s)}$, $WO_{3(l)}$
WO_3	1627	Decomposition	$WO_{3(l)}$, $WO_{2(l)}$,$O_{2(g)}$
WO_2	1730	Decomposition	$WO_{2(l)}$, $W_{(s)}$, $O_{2(g)}$
MoO_3	802	Melting	$MoO_{3(s)}$, $MoO_{3(l)}$
MoO_3	1155	Vaporization	$MoO_{3(l)}$, $MoO_{3(g)}$
Bi_2O_3	279	Melting	$Bi_2O_{3(s)}$, $Bi_2O_{3(l)}$
Bi_2O_3	1344	Decomposition	$Bi_2O_{3(l)}$,$Bi_{(l)}$ $O_{2(g)}$

Fig. 4givesthetemperatureevolutionas a functionoftheextentofreactionandfor all

consideredthermites, Al/CuO, Al/Sb_2O_3, Al/Bi_2O_3, $Al/MoO_3$and Al/WO_3.

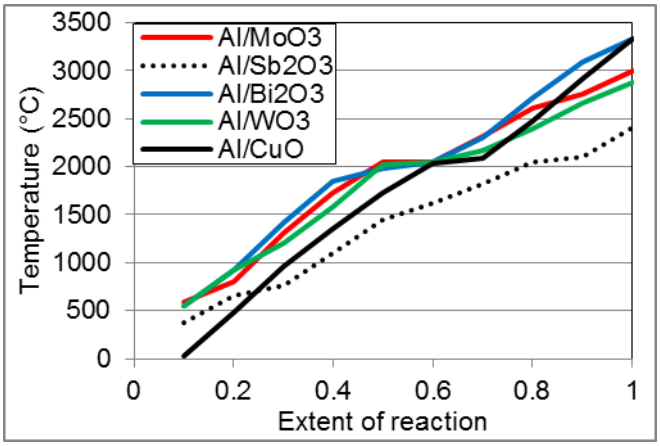

Fig. 4: Theoretical temperature as a function of extent of reaction,for Al/CuO,Al/WO_3, Al/Bi_2O_3, $Al/Sb_2O_3$and Al/MoO_3thermites.

If the overall curve shapes are almost linearly growing, they still exhibit different regimes separated by plateaus that correspond to the different phase transitions. Curves show that the maximum temperatures for all thermitesreaction reach roughly 3000 °C. The highesttemperature values are obtained for Al/CuO and Al/Bi_2O_3(3330°Cand 3327°C respectively reached at **ξ** = 1, i.e. complete reaction).Sb_2O_3,which has thelowestspecific heat of combustion, shows the lowest curve slope compared to the others, leading to the lowest final temperature 2411 °C.

Fig. 5 (a) (b) (c) and (d) give the maximum pressures as a function of the extent of reaction, for three TMD percentages (10, 30 and 50 %TMD) and for Al/Bi_2O_3, $Al/MoO_3Al/Sb_2O_3$ and Al/WO_3, respectively. The temperature variations are also presented for each thermite.

All thermites generate pressure and the maximum pressure is obtained at 50 %TMD for Al/Bi_2O_3 thermite (280 MPa at ξ = 0.6) followed by Al/MoO_3 mixture (220 MPa at ξ = 0.5).Al/WO_3 and Al/Sb_2O_3 produce both around 150 MPa during their reaction.

The general pressure curve shapes are similar for all thermites: a succession of peaks corresponding to the evaporation or decomposition onsets of various species, depending on the nature of the thermite and its associated chemistry. The origin of the peaks corresponds to the generation of gaseous species during thermite reaction,according tophase transitions (*(l)→(g) as well as (s)→(g)*) at equilibrium, as described in the section 2.

Considering Al/Bi_2O_3 (see Fig. 5.a), we observe first a decomposition of the bismuthoxide into molecular oxygen (O_2) and liquid bismuth occurring at ξ =0.6 and around 2041 °C. The Bi_2O_3 decomposition produces a pressure peak ranging from 32 MPa to 280 MPa,depending on TMD percentage. Thispressure peak is followed by the evaporation of Bi at ξ = 0.8, which corresponds to the gentle pressure shoulder especially visible at 50 %TMD.

For Al/MoO_3 (see Fig. 5.b), we observe first the vaporization of condensed MoO_3 into molecular $MoO_{3(g)}$ at ξ =0.5 leading to an important increase of the pressure: principal pressure peak of 221 MPa at 50% TMD. At the same time, the temperature rises rapidly leading to the decomposition of alumina (at ~2977°C) into $Al_{(g)}$+ O_2 occurring at ξ =0.8. At this temperature, Mo is still in a liquid phase. Moreover, only a small fraction of liquid alumina is decomposed at this stage. As a result, the final theoretical pressure is very low and only of0.5 MPa.This results from the low final temperature reached at complete reaction. One would expect a higher final temperature since Al/MoO_3 is more energetic than Al/Bi_2O_3 where decomposition of alumina is observed. The lowering of the temperature in the case of Al/MoO_3 is due to the higher heat capacity of Mo compared to Bi making it absorbing more energy.

For Al/Sb_2O_3 (see Fig. 5 c), the decomposition of Sb_2O_3 and the vaporization of Sb are respectively at 1425 °C and 1314°C (see Table 2). Not only the two peaks are very closeand collapse, but also Sb vaporization precedes Sb_2O_3decomposition such that almost all Sb produced should immediately evaporate. The result is that only one peak is clearly visible in Fig. 5 c.At the final stage of reaction, no alumina can be decomposed since the final temperature of 2411°C is well below alumina vaporization temperature. But, all Sb metal is vaporized leading to a pressure of 37MPa (at 50 %TMD).

For Al/WO_3 (see Fig. 5 d), the phase transformation leading to pressure generation are the decomposition of WO_3 into WO_2 and O_2 at 1625°C and then into $W_{(l)}$ and O_2 at 1730°C(see Table 2). After this point, the pressure decreases and falls to0.06 MPa At the final temperature of 2870°C, neither $W_{(l)}$nor $Al_2O_{3(l)}$ can be vaporized.

To conclude this section we can state that the best alumino-thermite material to generate pressure is not necessarily the most energetic thermite, here Al/CuO, but the one with the oxide whose metal evaporates easily and where temperature allows for alumina decomposition: here Al/Bi_2O_3.

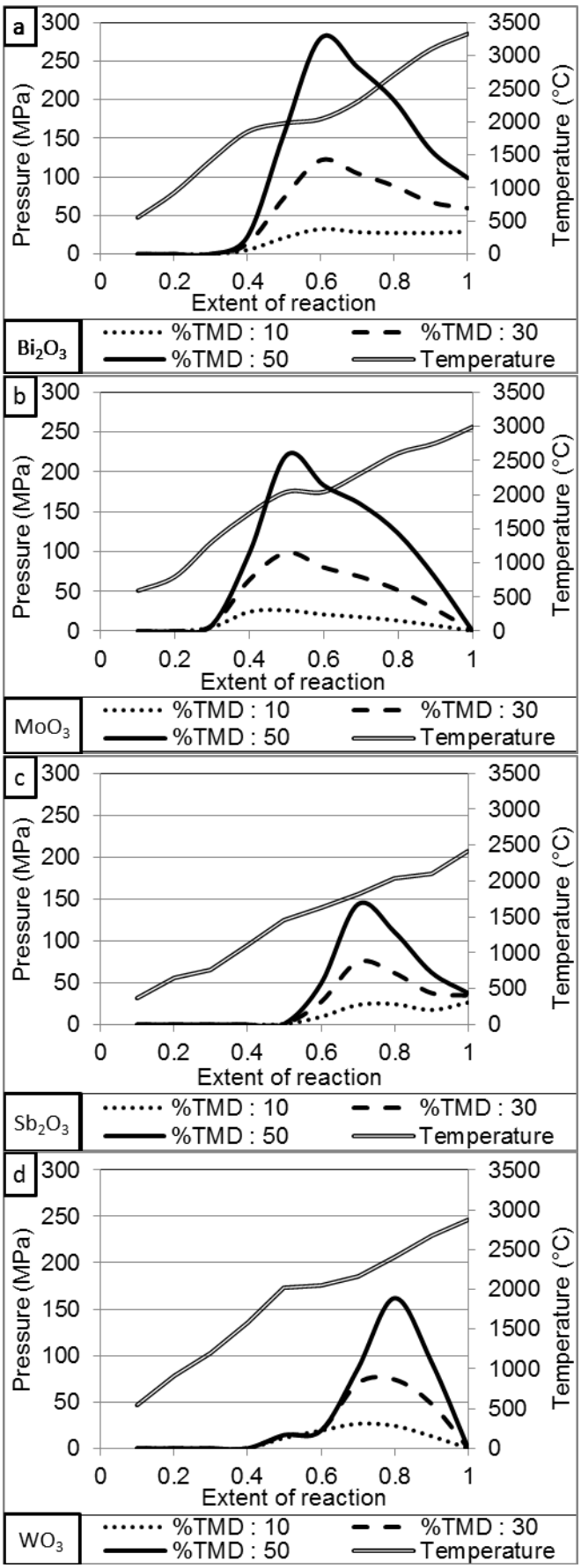

Fig. 5: Theoretical pressure, for different %TMD, and the temperature as a function of extent of reaction,for Al/Bi_2O_3 (a), Al/MoO_3 (b), Al/Sb_2O_3(c) and Al/WO_3(d).

4 Experimental validationand discussion

Theoretical results were compared to experimental data in order to evaluate their validity. For that purpose, stoichiometric Al/oxide thermites were prepared by ultrasonic mixing. The maximum pressure generated by the exothermic reaction was measured for each couple.

4.1 Materials

The Al nanoparticles, with a diameter of 80 nm, are supplied by Novacentrix.They exhibited spherical shapes and the purity has been measured at 68 % leading to an alumina shell thickness of 4 nm. Bi_2O_3, CuO, MoO_3, WO_3 and Sb_2O_3 oxide nanopowders are supplied by SigmaAldrichwith characteristics summarized in Table 3.

Table 3: Summary of powders used in the nanothermites mixture.

Element	Manufacturer	Measured size	Shape
Al	Novacentrix	80 - 150 nm	Spherical
Bi_2O_3	SigmaAldrich	100 - 500 nm	Ovoid
MoO_3	SigmaAldrich	90 - 6000 nm	Random shape
CuO	SigmaAldrich	240 nm +/- 50 nm	Random shape
Sb_2O_3	SigmaAldrich	120 - 4200 nm	Random shape

The Al and oxidizer nanopowderswere mixed in stoichiometric ratios, taking the fractional alumina content into account. The Al/oxide ratios in the mixture are of 35.5 wt. %, 15 wt. %, 24.6 wt. % and 21.4 wt. % for Al/MoO_3, Al/Bi_2O_3, Al/CuO and Al/Sb_2O_3 mixtures, respectively. First, Al and oxidizer nanopowders were weighted, suspended in hexane and then mixed with an ultrasonic rod style transducer for a total of 4.5 min with a 1 s delay after every 2 s of sonication to avoid heating the solution that could lead to undesired ignition of mixture. The mixture suspension was then dried at 70°C under 2.10^4 Pa and collected for pressure characterization.

4.2 Characterization set-up

The pressure released by the reaction was measured in a stainless steel, high pressure resistant (up to 100 MPa) cylindrical reactor. The reactor has 4 mm inner diameter and is 0.7 mm long (total volume of ~ 9 mm^3). A pressure up to 100 MPa can be measured by a high-frequency pressure transducer (Kistler 601H) on the back of the reactor and connected to a Kistler charge amplifier (5018 type). A schematic is shown in Fig. 6. Densities were calculated based on the reactor volume and the mass of powder loaded inside. For each sample, 10, 30 and 50 %TMD were systematically investigated. For ignition, we used a multilayer nanothermite Al/CuO on a chip[16].

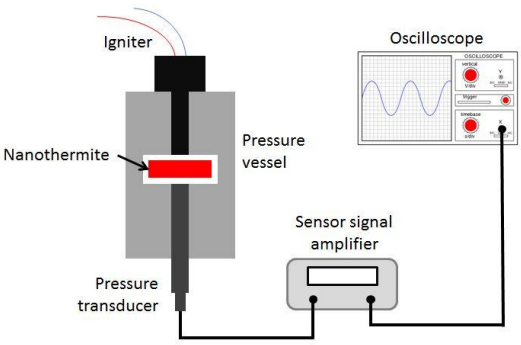

Fig. 6: Schematic view of the experimental pressure measurement set up.

4.3 Discussion

Fig. 7 gives a comparison of simulated and experimental pressures at completed reaction for Al/Bi_2O_3, Al/MoO_3,Al/Sb_2O_3 and Al/CuO respectively and for the three different TMD percentages: 10, 30 and 50 %TMD. As in the simulations, experimental measurements indicate that all thermites produce pressure. At 30 and 50 %TMD, thermites can be divided into two groups. Al/CuO and Al/Bi_2O_3 exhibit the highest pressures, from 20 to 40 MPa, while as expected Al/Sb_2O_3 and Al/MoO_3 generate less gas with pressures ranging from 7 to 15 MPa.

For Al/CuO, Al/Sb_2O_3 and Al/Bi_2O_3 theoretical results overestimate the pressure with respect to experiments. The best fit between modeling and simulation is obtained for Al/CuO with a model/experimental results agreement within a factor of 3, while in [35], the pressures were overestimated by one order of magnitude. The main reason for this improvement is that the chemical processes occurring in Al/CuO combustion are well known and documented.

Experimentally, the highest pressure is obtained at 50%TMD for Al/CuO followed by Al/Bi_2O_3, Al/Sb_2O_3 and Al/MoO_3: 29 MPa, 15 MPa and 12 MPa respectively.

At 10 %TMD(see Fig. 7), our calculations show that Al/Sb_2O_3 produces more pressure than Al/CuO. But, its low pressure increase with TMD leads to lower pressures for 30 and 50 %TMD, compared to Al/CuO. We observe the same trend experimentally: at 10 TMD percentage, the Al/Sb_2O_3 experimental pressure reaches 4.4 MPa, very close even if still lower than Al/CuO thermite 5.1 MPa.Increasing the TMD percentage, the experimental pressure increases slowly to reach 15 MPa for Al/Sb_2O_3, well below Al/CuO pressure that stabilizes at 42 MPa.

The overestimation of pressure for Al/Bi_2O_3 and Al/Sb_2O_3 thermites is due to the easy evaporation of Bi and Sb atoms in the respective thermites. The assumption of the gas phase containing metals in atomic form, adopted in our model, is probably not accurate. The metal should aggregate thus decreasing the calculated pressures.

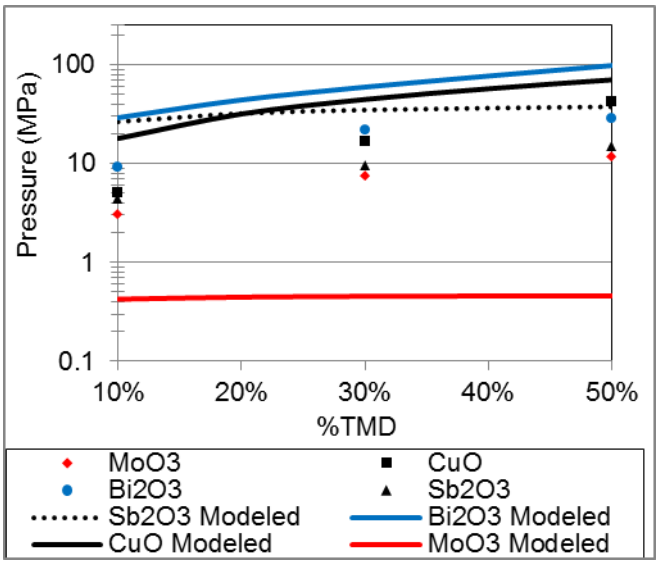

Fig. 7: Comparison of simulated and experimental pressures at completed reaction for Al/MoO_3,Al/CuO, Al/$Bi_2O_3$and Al/Sb_2O_3 for three %TMD: 10%, 20% and 50%.

In contrast to all other cases, the pressures calculated for Al/MoO_3 thermite are well below experimental ones: at 50 %TMD the calculation gives 0.5MPa instead of 12 MPa measured. As stated in section 3, the highest temperatures of Mo vaporization and alumina decomposition are not reached during combustion so that all the end products are found in condensed form, leaving a residual pressure of 0.5 MPa at the end of the reaction.

The discrepancy between experimental and theoretical pressures may be attributed to three effects: (1) the expected composition of the final gas phase, (2) the chemical processes in condensed phase and (3) the real kinetic effects. First, the complexity of the gas phase is difficult to grasp. In the present paper, we consider that vaporization processes lead only to the formation of gas phases constituted of individual metallic atoms or O_2 molecules, except for MoO_3 where the existence of molecular gas is well known. Obviously, this assumption that completely neglects the potential formation of metallic aggregates in the gas phase, and the associated condensation properties, will lead to an overestimation of pressures. For example, it is probable that Bi will preferentially form Bi_2 molecules. For what concerns Sb_2O_3 decomposition, it is suggested that liquid Sb_2O_3will evaporateas Sb_4O_6molecules[39]. All these reactions are not sufficiently documented to allow a precise treatment in our modeling procedure.

Second, the chemical processes are not limited to the gas phase, but may also occur in the condensed

phase. Apart from the trivial melting of solids, already taken into account in our present model, one can observe solid-to-solid phase transitions, stoichiometry variations, alloying in solid phase and mixing in liquid phase. An example is the formation of AlCu alloy during Al/CuO thermite combustion. AlCu alloy is actually found in combustion residues, but no more detail upon its formation is presently available. Given the range of temperatures scanned, such processes may happen very frequently. An accurate representation of these processes needs also a thorough study using quantum chemical calculations.

Our intention in the present paper is not to speculate on the chemistry of phase transitions, but rather to demonstrate the possibility of establishing a generic model predicting the maximal pressure and temperature for combustion of thermite depending on the available thermodynamic data. Further insights on the phase transitions chemistries, in condensed or gas phase can be unraveled and quantified properly from first principles quantum chemistry calculations.

Finally, the explicit time dependence of the reactions is a major source of discrepancies. The experimental rising times of the pressure in the combustion chamber are always less than 1 ms. The approximation of local thermodynamic equilibrium, leading to the concept of extent of reaction, is only a rough approximation. A kinetic approach, substituting the real time variable to the extent of reaction, is under development. This approach would enable us to consider transient metastable species, which may appear, more or less briefly, in the combustion chamber. These species may not of long lifetimes, but will have a significant importance on the pressure evolution. For example, aggregates of various sizes shall momentarily decrease the pressure, and disappear rapidly, forming new species. If the thermodynamic of these aggregates is well documented, through quantum calculations or experiments, they can be easily incorporated in our kinetic approach.

5 Conclusion

A local thermodynamics equilibrium model describing the pressure generation through reaction of various aluminum-based thermites is established in this paper.
The model includes the determination of partial pressures as a function of condensation temperatures. It allows determining the partial pressures of gas phase reactants as well as the total pressure reached during and up to the complete reaction process (i.e. as a function of the extent of reaction). It also makes it possible to study the pressure delivered as a function of the compaction rate (%TMD). We applied our model to some commonly used thermite compositions, namely Al/CuO, Al/MoO_3, Al/WO_3, Al/Bi_2O_3 and Al/Sb_2O_3. We observe that the highest final pressure is obtained for Al/CuO and Al/Bi_2O_3 couples, mainly due to the partial decomposition of liquid alumina since the heat of reaction permits to reach high final reaction temperature, 3330°C and 3327 °C for Al/CuO and Al/Bi_2O_3, respectively.
Simulations are compared to experiment for validation purpose. The final pressures predicted by the model are in fair agreement with experimental values. However, details on the mechanisms of gas generation are obtained such as the two-stage growth regime of the total pressure generated during reaction of Al/CuO, which has been observed experimentally. We should emphasize that all the parameters in the model are taken from thermodynamic data in the literature. No adjustable parameter, to be fitted to validation experiments, is used in the model. In order to improve our model quantitatively, without introducing adjustable parameters, future work is required, specifically by investigating the chemistry of the reactants in both the condensed and gas phases.

ACKNOWLEDGEMENTS

This work has been supported by CNRS with the contribution of DGA. The authors wish to thanks the DGA (French general delegation of armament) for their support.

References

[1] D. Stamatis, X. J. Jiang, E. Beloni, and E. L. Dreizin, Aluminum Burn Rate Modifiers Based on Reactive Nanocomposite Powders, *Propellants Explosives Pyrotechnics*, Jun **2010,** *35*, 260-267.

[2] D. A. Reese, S. F. Son, and L. J. Groven, Preparation and Characterization of Energetic Crystals with Nanoparticle Inclusions, *Propellants Explosives Pyrotechnics,*Dec **2012,** *37*, 635-638.

[3] H. Y. Wang, G. Q. Jian, S. Yan, J. B. DeLisio, C. Huang, and M. R. Zachariah, Electrospray Formation of Gelled Nano-Aluminum Microspheres with Superior Reactivity, *Acs Applied Materials & Interfaces*, Aug 14 **2013,***5*, 6797-6801.

[4] W. Churaman, L. Currano, and C. Becker, Initiation and reaction tuning of nanoporous energetic silicon, *Journal of Physics and Chemistry of Solids,* Feb **2010,***71*, 69-74,.

[5] F. Zhang, Y. L. Wang, D. X. Fu, L. M. Li, and G. F. Yin, In-situ Preparation of a Porous Copper Based Nano-Energetic Composite and Its Electrical Ignition Properties, *Propellants Explosives Pyrotechnics*, Feb **2013,** *38*, 41-47.

[6] S. X. Wang, R. Q. Shen, Y. H. Ye, and Y. Hu, An investigation into the fabrication and combustion performance of porous silicon nanoenergetic array chips, *Nanotechnology*, Nov 2 **2012,** *23*.

[7] K. L. Zhang, C. Rossi, M. Petrantoni, and N. Mauran, A nano initiator realized by integrating Al/CuO-based nanoenergetic materials with a Au/Pt/Cr microheater, *Journal*

ofMicroelectromechanical Systems, Aug **2008,***17*, 832-836.

[8] C. J. Morris, B. Mary, E. Zakar, S. Barron, G. Fritz, O. Knio*, et al.*, Rapid initiation of reactions in Al/Ni multilayers with nanoscale layering, *Journal of Physics and Chemistry of Solids*, Feb **2010,** *71*, 84-89.

[9] X. Zhou, R. Q. Shen, Y. H. Ye, P. Zhu, Y. Hu, and L. Z. Wu, Influence of Al/CuO reactive multilayer films additives on exploding foil initiator, *Journal of Applied Physics*, Nov 1 **2011,** *110*.

[10] P. Zhu, R. Q. Shen, Y. H. Ye, X. Zhou, and Y. Hu, Energetic igniters realized by integrating Al/CuO reactive multilayer films with Cr films, *Journal of Applied Physics*, Oct 1 **2011,***110*.

[11] C. J. Morris, P. Wilkins, C. May, E. Zakar, and T. P. Weihs, Streak spectrograph temperature analysis from electrically exploded Ni/Al nanolaminates, *Thin Solid Films*, Dec 30 **2011,***520*, 1645-1650.

[12] C. S. Staley, C. J. Morris, R. Thiruvengadathan, S. J. Apperson, K. Gangopadhyay, and S. Gangopadhyay, Silicon-based bridge wire micro-chip initiators for bismuth oxide-aluminum nanothermite, *Journal of Micromechanics and Microengineering*, Nov **2011,***21*.

[13] X. T. Qiu, R. Tang, R. R. Liu, H. Huang, S. M. Guo, and H. Y. Yu, A micro initiator realized by reactive Ni/Al nanolaminates, *Journal of Materials Science-Materials in Electronics*, Dec **2012,***23*, 2140-2144.

[14] C. Yang, Y. Hu, R. Q. Shen, Y. H. Ye, S. X. Wang, and T. L. Hua, Fabrication and performance characterization of Al/Ni multilayer energetic films, *Applied Physics a-Materials Science & Processing*, Feb **2014,***114*, 459-464.

[15] C. J. Morris, P. R. Wilkins, and C. M. May, Streak spectroscopy and velocimetry of electrically exploded Ni/Al laminates, *Journal of Applied Physics*, Jan 28 **2013,***113*.

[16] G. Taton, D. Lagrange, V. Conedera, L. Renaud, and C. Rossi, Micro-chip initiator realized by integrating Al/CuO multilayer nanothermite on polymeric membrane, *Journal of Micromechanics and Microengineering*, Oct **2013,***23*.

[17] P. Zhu, R. Q. Shen, Y. H. Ye, S. Fu, and D. L. Li, Characterization of Al/CuO nanoenergetic multilayer films integrated with semiconductor bridge for initiator applications, *Journal of Applied Physics*, May 14 **2013,***113*.

[18] C. H. Lee, T. H. Jeong, D. K. Kim, W. H. Jeong, M. K. Kang, T. H. Hwang*, et al.*, Crystallization of amorphous silicon thin films using nanoenergetic intermolecular materials with buffer layers, *Journal of Crystal Growth*, Feb 1 **2009,***311*, 1025-1031.

[19] J. H. Bae, D. K. Kim, T. H. Jeong, and H. J. Kim, Crystallization of amorphous Si thin films by the reaction of MoO3/Al nanoengineered thermite, *Thin Solid Films*, Sep 1 **2010,***518*, 6205-6209.

[20] M. Hossain, S. Subramanian, S. Bhattacharya, Y. F. Gao, S. Apperson, R. Shende*, et al.*, Crystallization of amorphous silicon by self-propagation of nanoengineered thermites, *Journal of Applied Physics*, Mar 1 **2007,***101*.

[21] C. Rossi, K. Zhang, D. Esteve, P. Alphonse, P. Tailhades, and C. Vahlas, Nanoenergetic materials for MEMS: A review, *Journal of Microelectromechanical Systems*, Aug **2007,** *16*, 919-931.

[22] S. H. Fischer and M. C. Grubelich, Theoretical energy release of thermites, intermetallics, combustible metals,, *in Proc. 24th Int. Pyrotechnics Seminar, Monterey, CA, Jul.* **1998***, 1–6*.

[23] G. A. A. Rodriguez, S. Suhard, C. Rossi, D. Esteve, P. Fau, S. Sabo-Etienne*, et al.*, A microactuator based on the decomposition of an energetic material for disposable lab-on-chip applications: fabrication and test, *Journal of Micromechanics and Microengineering*, Jan **2009,***19*.

[24] M. Korampally, S. J. Apperson, C. S. Staley, J. A. Castorena, R. Thiruvengadathan, K. Gangopadhyay*, et al.*, Transient pressure mediated intranuclear delivery of FITC-Dextran into chicken cardiomyocytes by MEMS-based nanothermite reaction actuator, *Sensors and Actuators B-Chemical*, Aug-Sep **2012,** *171*, 1292-1296.

[25] K. T. Sullivan, C. W. Wu, N. W. Piekiel, K. Gaskell, and M. R. Zachariah, Synthesis and reactivity of nano-Ag2O as an oxidizer for energetic systems yielding antimicrobial products, *Combustion and Flame*, Feb **2013** *160*, 438-446.

[26] S. A. Grinshpun, A. Adhikari, M. Yermakov, T. Reponen, E. Dreizin, M. Schoenitz*, et al.*, Inactivation of Aerosolized Bacillus atrophaeus (BG) Endospores and MS2 Viruses by Combustion of Reactive Materials, *Environmental Science & Technology*, Jul 3 **2012,***46*, 7334-7341.

[27] B. R. Clark and M. L. Pantoya, The aluminium and iodine pentoxide reaction for the destruction of spore forming bacteria, *Physical Chemistry Chemical Physics*, **2010,***12*, 12653-12657.

[28] M. Q. Fan, F. Xu, and L. X. Sun, Studies on hydrogen generation characteristics of hydrolysis of the ball milling Al-based materials in pure water, *International Journal of Hydrogen Energy*, Sep **2007,***32*, 2809-2815.

[29] P. Dupiano, D. Stamatis, and E. L. Dreizin, Hydrogen production by reacting water with mechanically milled composite aluminum-metal oxide powders, *International Journal of Hydrogen Energy*, Apr **2011,***36*, 4781-4791.

[30] K. S. Martirosyan, L. Wang, A. Vicent, and D. Luss, Synthesis and performance of bismuth trioxide nanoparticles for high energy gas generator use, *Nanotechnology*, Oct 7 **2009,***20*.

[31] K. S. Martirosyan, L. Wang, and D. Luss, Novel nanoenergetic system based on iodine pentoxide, *Chemical Physics Letters*, Nov 24 **2009,***483*,107-110.

[32] S. Chowdhury, K. Sullivan, N. Piekiel, L. Zhou, and M. R. Zachariah, Diffusive vs Explosive Reaction at the Nanoscale,*J. Phys. Chem. C*, May **2010**, *114*(20), 9191–9195.

[33] L. Zhou, N. Piekiel, S. Chowdhury, and M. R. Zachariah, Time-Resolved Mass Spectrometry of the Exothermic Reaction between Nanoaluminum and Metal Oxides: The Role of Oxygen Release,*J. Phys. Chem. C*, Aug. **2010**, *114*(33), 14269–14275.

[34] K. S. Martirosyan, M. Zyskin, C. M. Jenkins, and Y. Horie, Modeling and simulation of pressure waves generated by nano-thermite reactions, *Journal of Applied Physics*, **2012,***112*, 094319 - 094319-9**.**

[35] L. Glavier, G. Taton, J.-M. Ducere, V. Baijot, S. Pinon, T. Calais, et al., NanoEnergetics as pressure generator for nontoxic impact primers: comparison of Al/Bi2O3, Al/CuO, Al/MoO3 nanothermites and Al/PTFE, *Combustion and Flame*, **2015,** vol. In progress.

[36] D. R. Lide, *Handbook of Chemistry and Physics*, *87th ed.: CRC Press*, Taylor & Francis, **2006-2007**.

[37] C. Boissière and G. Fiorese, Équation d'état des métaux prenant en compte les changements d'état entre 300 et 200 000 K pour toute compression. Application au cas du cuivre et de l'aluminium, *Rev. Phys. Appl.* (Paris), **1977,** *12*, 857-872.

[38] P. Zhang, R. Chang, Z. Wei, H. Cao, and X. Zhou, The melting-point, latent-heat of solidification, and enthalpy for both solid and liquid alpha-Al2O3 in the range 550-2400 K, *International Journal of Thermophysics*, Jul **1986,***7*, 811-819.

[39] N. A. Asryan, A. S. Alikhanyan, and G. D. Nipan, p-T-x phase diagram of the Sb-O system, Inorganic Materials, Jun **2004,***40*, 626-631.

Received: ((will be filled in by the editorial staff))
Revised: ((will be filled in by the editorial staff))